FALSE BOTTOM EFFECT ON THE HYDRODYNAMIC FORCES ACTING ON A SHIP HULL DURING AN OBLIQUE TOWING TEST AND COUNTERMEASURES

Yosuke Hachiya, Masaaki Sano and **Ryusuke Okuda,** Hiroshima University, Hiroshima, Japan
Yoshitaka Furukawa, Kyushu University, Fukuoka, Japan
Hironori Yasukawa, Hiroshima University, Hiroshima, Japan

SUMMARY

The difference in the manoeuvring hydrodynamic forces acting on a ship model measured in a false bottom and true bottom should be concerned for the measurement accuracy. Therefore, this study investigated the effect of the false bottom in shallow water during an oblique towing test. First, to capture the effect of the false bottom, oblique towing tests were conducted using a KRISO Container Ship (KCS) model in a towing tank with a false bottom and a rectangular shallow water tank with a true bottom. The experimental results showed that the lateral force and yaw moment in the false bottom condition became smaller than those in the true bottom condition with decreasing water depth. Next, a computational fluid dynamics (CFD) simulation was conducted to clarify the mechanism of the observed decrease in the hydrodynamic forces acting on the ship model in the false bottom condition. Finally, countermeasures against the effect of the false bottom were proposed and preliminary investigated using CFD.

NOMENCLATURE

B	Ship breadth (m)
B_f	Breadth of the false bottom (m)
C_b	Block coefficient (-)
C_p	Pressure coefficient (-)
c_1	Correction coefficient with respect to $\beta_{\mathrm{Effective}}$ (-)
d	Ship draft (m)
F_n	Froud number based on ship length (-)
h	Depth of water (m)
L_{pp}	Ship length between perpendiculars (m)
N	Yaw moment around midship (N m)
o-xyz	Ship fixed coordinate systems taking the origin at midship
o_0-$x_0y_0z_0$	Inertial coordinate systems which move in parallel at the ship speed
p	Pressure (N/m^2)
U	Ship speed (m/s)
u	Surge velocity (m/s)
u_x	Flow velocity in x_0 direction (m/s)
u_y	Flow velocity in y_0 direction (m/s)
v_m	Lateral velocity at midship (m/s)
X	Surge force of a ship (N)
x_G	Longitudinal coordinate of centre of gravity (m)
Y	lateral force of a ship (N)
β	Drift angle (rad)
$\beta_{\mathrm{Effective}}$	Effective drift angle (rad)
∇	Displacement volume of ship (m^3)
ΔY	Longitudinal distribution of lateral force (N/m)
ρ	Density of water (kg/m^3)
$'$	Non-dimensional quantity (-)

1 INTRODUCTION

Ship navigation in a harbour or canal is a critical phase because accidents are more likely to occur in shallow water. Therefore, ship manoeuvrability in shallow water must be predicted accurately, and a great deal of research has been conducted accordingly (Fujino et al., 1984; Vantorre et al., 2017). One of the more practical methods of studying shallow water effects is the tank test using a ship model. However, few tanks are able to adjust the actual water level to conduct model tests in shallow water owing to the constraints of the tank structure. Thus, tanks for shallow water tests often use a temporary, artificial bottom, called a "false bottom", as opposed to the actual bottom of the tank, which is referred to as the "true bottom." Although this approach is convenient and efficient, it has been shown that the manoeuvring hydrodynamic forces acting on a ship model in a false bottom condition are different from those acting on a model in a true bottom condition. For example, Sakamoto et al. (2020) conducted an oblique towing test using viscous CFD simulations to investigate the effect of the false bottom on the hydrodynamic forces through the comparison with the experimental results. They observed that the lateral force and yaw moment in the static drift condition were smaller with the false bottom than with the true bottom. Furthermore, Sakamoto et al. (2021) continued to investigate the effect of the false bottom on yaw-related hydrodynamic forces based on pure yawing tests using CFD simulations. Investigating the effect of the false bottom on manoeuvring hydrodynamic forces was further addressed by the 29th ITTC (2021) as an important issue. This topic is called the "false bottom effect" in this study. Because the Hiroshima University towing tank also uses a false bottom, a systematic investigation of the false bottom effect considering various water depths and drift angles is required. Moreover, some countermeasures against the false bottom effect should also be concerned.

This study therefore investigated the false bottom effect on the hydrodynamic forces acting on an obliquely moving ship model. First, oblique towing tests were conducted in a false bottom tank and a true bottom tank. The test with the false bottom was conducted in the Hiroshima University towing tank. The test with the true bottom was con-

ducted in the Kyushu University seakeeping and manoeuvring basin. In these tests, a KCS model with a length L_{pp} = 3.057 was used. The ratio of water depth to draft (h/d) was varied from 1.5 to 1.3 to 1.2. Next, CFD simulations were conducted using the same conditions as the experiments. The pressure and flow field in the false bottom condition were compared to those in the true bottom condition, and the mechanism of the false bottom effect is discussed in this paper accordingly. Finally, countermeasures against the false bottom effect were proposed and preliminary investigated using CFD.

2 EXPERIMENTAL STUDY ON THE FALSE BOTTOM EFFECT

2.1 EXPERIMENTAL TANK

In this study, captive model tests were conducted in shallow water using two types of tank bottoms to investigate the false bottom effect on the hydrodynamic forces acting on an obliquely moving ship model.

2.1 (a) False bottom experiment

The false bottom tank test was conducted in the Hiroshima University towing tank (length 100 m, width 8 m, maximum depth 3.5 m). Figure 1 shows a photograph of the tank, which has a false bottom with a width of $B_f = 5$ m. Shallow water model tests can be conducted by adjusting the height of this false bottom, but only in the centre of the tank, as the false bottom does not extend to the full width or length of the tank.

Figure 1. Photograph of the Hiroshima University towing tank equipped with a false bottom

2.1 (b) True bottom experiment

The true bottom tank test was conducted in the Kyushu University seakeeping and manoeuvring basin (length 38.8 m, width 24.4 m, maximum depth 2 m). Figure 2 shows a photograph of this tank, in which shallow water model tests can be conducted by changing the volume of water. Thus, the entire tank provides a shallow water area, unlike the false bottom tank.

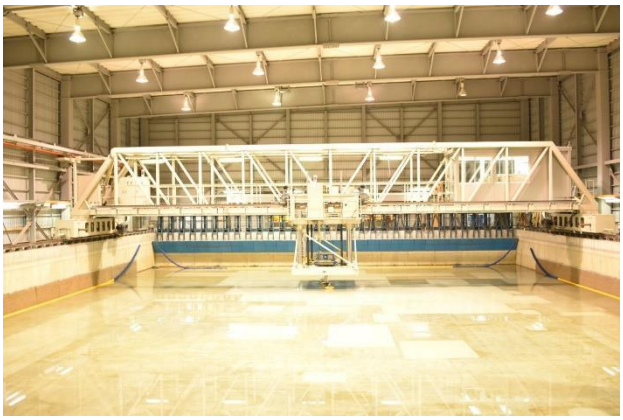

Figure 2. Photograph of the Kyushu University seakeeping and manoeuvring basin (true bottom)

2.2 SUBJECT SHIP MODEL

The KCS (SIMMAN, 2008) was selected as the subject ship model in this study. Figure 3 shows a photograph of the ship model used in these experiments. Table 1 provides the principal particulars of the full-scale and model-scale ships. In this study, the bare hull was employed without the rudder or propeller.

Figure 3. A photograph of KCS model

Table 1. Principal particulars of the KCS model ship

Symbol	Full scale	Model scale
Scale	1:1	1:75.237
L_{pp} [m]	230	3.057
B [m]	32.2	0.428
d [m]	10.8	0.144
∇ [m^3]	52043	0.122
x_G [m]	-3.404	-0.045
C_b	0.651	0.651

2.3 COORDINATE SYSTEMS AND TEST CONDITIONS

The coordinate systems used in the present study are shown in Figure 4. The space-fixed coordinate system is denoted as o_0-$x_0y_0z_0$, where o_0 is located at the centre of the tank and midship, the x_0-y_0 plane coincides with the still water surface, and the z_0 axis points vertically downward. The moving ship-fixed coordinate system is denoted as o-xyz, where o is located at midship, the x-y plane coincides with the still water surface, and the x, y, and z axes point toward the ship's bow, starboard, and vertically downwards, respectively. The total velocity U is expressed as $U = \sqrt{u^2 + {v_m}^2}$, where u and v_m indicate the velocity components at midship in the x and y directions, respectively. The drift angle β is defined as the angle between U and the x axis, as show in Figure 4, and is expressed as $\beta = \tan^{-1}(-v_m/u)$.

Table 2 shows the experimental conditions of the captive model tests. The Froude number was set to F_n = 0.095, equivalent to a ship speed of 8.75 knots at full-scale ship, and β was changed from -15° to +15° in 3° intervals. The water depth to ship draft ratio h/d was changed from 1.5 to 1.3 to 1.2. During the tests, heave and pitch motions were free but roll motion was fixed. The surge force X, lateral force Y, and yaw moment around midship N were measuered. These measured forces and moments were then non-dimensionalised using $(1/2)\rho L_{pp} dU^2$ and $(1/2)\rho {L_{pp}}^2 dU^2$, respectively, where ρ is the water density. A variable with a prime symbol, as in X', indicates the non-dimensional value of the variable.

2.4 FALSE BOTTOM EFFECT ON THE HYDRODYNAMIC FORCES ACTING ON AN OBLIQUELY MOVING SHIP MODEL

The hydrodynamic forces acting on an obliquely moving ship model in the false bottom condition were compared with those acting on the same ship in the true bottom condition to determine the false bottom effect on these forces. Figure 5, 6, and 7 show comparisons of the obtained non-dimensional surge force X', lateral force Y', and yaw moment N', respectively. The absolute value of X' measured in the false bottom condition with h/d=1.2 was larger than that measured in the true bottom condition when β was greater than 9°. However, X' is ten times smaller than Y', as shown by the vertical axis range in Figure 5 and 6. Thus, the difference between X' in the false bottom and true bottom conditions was insignificant compared to the difference between Y' and N' in each condition. The absolute values of Y' and N' in the false bottom condition were consistently smaller than those in the true bottom condition. This difference became increasingly significant with decreasing water depth from h/d=1.5 to 1.2. For example, the values of Y' and N' measured in the false bottom condition with h/d=1.2 at β=12° were 47% and 43% smaller, respectively, than those in the true bottom condition. These measured decreases in Y' and N' in the false bottom condition are similar to the results of the study by Sakamoto et al. (2020).

Since the tank width of Kyushu University was approximately three times wider than that of Hiroshima University, the effect of the tank width on the hydrodynamic forces was concerned. However, as discussed in the appendix, the difference of tank width does not seem to have significant impact on the hydrodynamic forces measured in this false-bottom area.

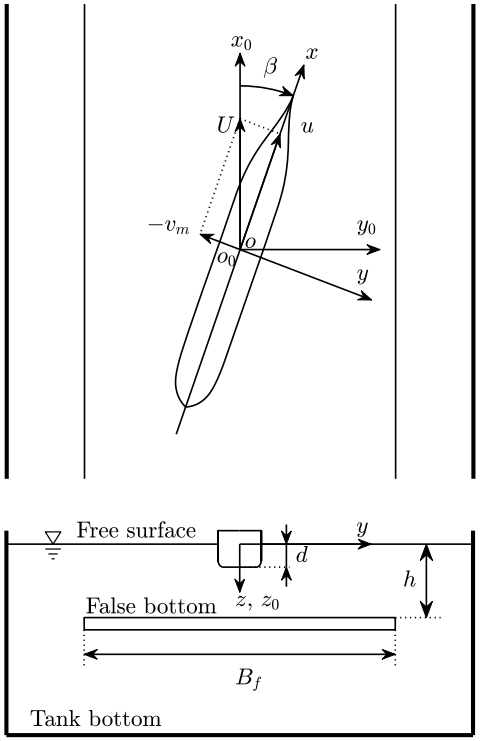

Figure 4. Coordinate systems

Table 2. Experimental oblique towing test conditions for KCS model

Parameter	Value
F_n	0.095
U [m/s]	0.519
β [°]	0, ±3, ±6, ±9, ±12, ±15
h/d	1.5, 1.3, 1.2
Bottom	False bottom / true bottom

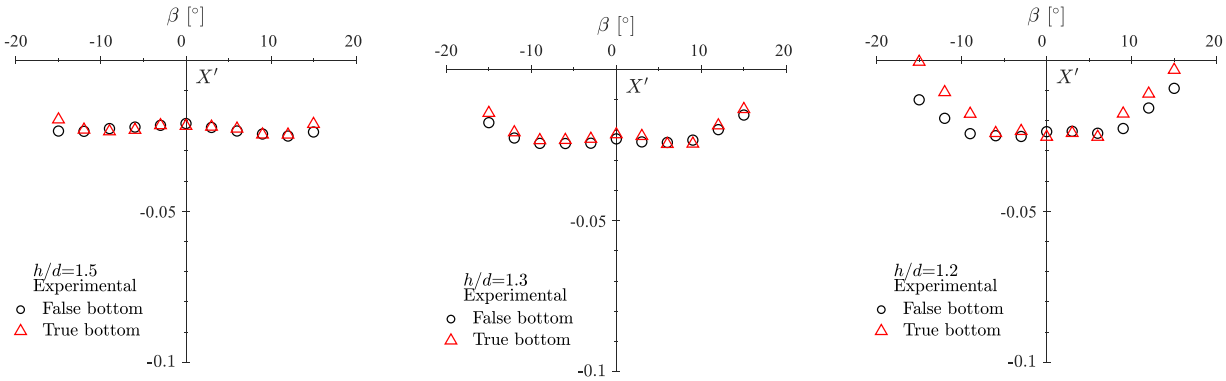

Figure 5. Comparison of the non-dimensional surge force obtained by the captive model tests in the false bottom and true bottom conditions at different water depths

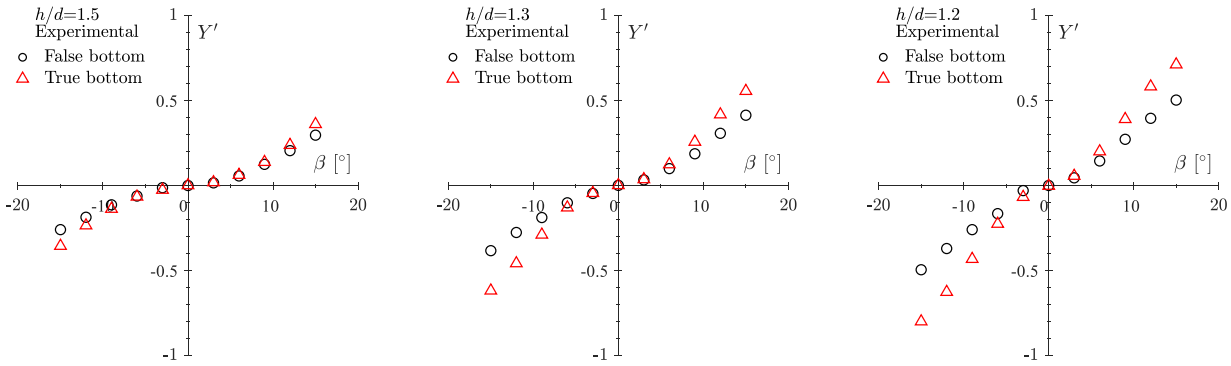

Figure 6. Comparison of the non-dimensional lateral force obtained by the captive model tests in the false bottom and true bottom conditions at different water depths

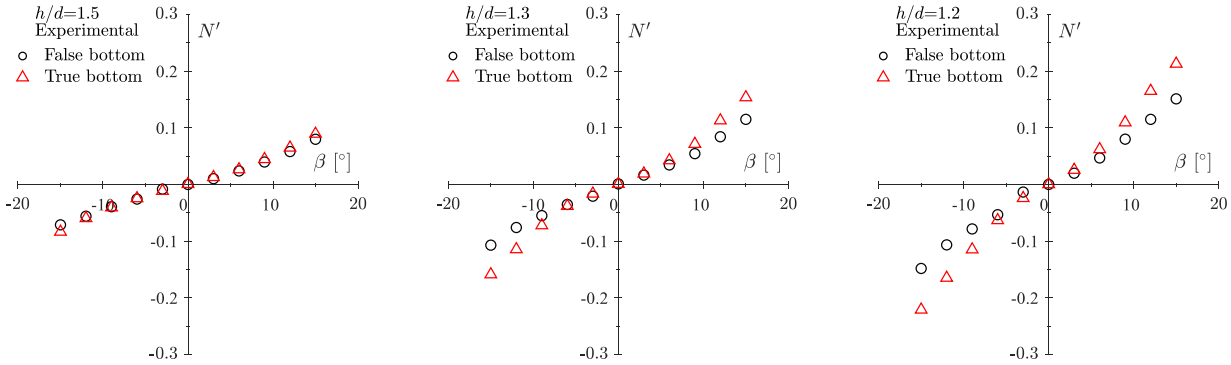

Figure 7. Comparison of the non-dimensional yaw moment around midship obtained by the captive model tests in the false bottom and true bottom conditions at different water depths

3 COMPUTATIONAL STUDY ON THE FALSE BOTTOM EFFECT

In this study, a CFD simulation was conducted to understand the mechanism underlying the false bottom effect. In this section, the computational results are first verified by comparison with the experimental results. Then, the false bottom effect is discussed using the computed flow field.

3.1 OUTLINE OF CFD SIMULATION

The OpenFoam software package (The OpenFOAM Foundation, 2016) was used for the CFD simulation in this study. In this section, the calculation settings are introduced.

The ITTC guidelines (the 29th ITTC, 2021) were used as a reference when establishing the computational domain, which is summarized in Table 3. The simulated tank widths were the same as those of the Hiroshima University towing tank (8 m) and the Kyushu University seakeeping and manoeuvring basin (24 m). The background grid was created using “blockMesh”, and the grid around the hull was refined using “snappyHexMesh”, which are applications included with OpenFoam.

In this study, a steady-state incompressible fluid turbulent flow analysis was conducted in the false bottom and rue bottom conditions. The pressure–velocity coupling was obtained using the SIMPLE algorithm in the numerical calculation. In this study, the $k-\omega$ shear stress transport (Menter et al., 2003) was selected as the turbulence model. The governing equations were spatially discretized using the second-order central differencing scheme for the diffusion term, and the first- and second-order upwind schemes for the advection term to stabilize the calculation.

Table 3. Summary of the computational domain

False bottom	True bottom
$-4.5 \leq x_0/L_{pp} \leq 2.5$	$-4.5 \leq x_0/L_{pp} \leq 2.5$
$-1.3 \leq y_0/L_{pp} \leq 1.3$	$-3.9 \leq y_0/L_{pp} \leq 3.9$
$0 \leq z_0/d \leq 24.4$	$0 \leq z_0/d \leq 1.5, 1.3, 1.2$

For the boundary conditions applied in the CFD simulations, the flow velocity corresponding to the ship speed was fixed at the inlet boundary and a no-slip wall moving at ship speed was applied to the tank bottom, tank side wall, and false bottom. Considering the low ship speed in the simulation, the effect of the free surface was expected to be negligible; thus, the double model assumption was applied, and the free surface was not considered. In the CFD simulation, the change in the running attitude of the hull (sinkage and trim) was not considered.

Table 4 shows the calculation conditions of the captive model test, which were the same as the experimental conditions (Table 2).

Table 4. Computational oblique towing test conditions for KCS model

Parameter	Value
F_n	0.095
U [m/s]	0.519
β [°]	0, 3, 6, 9, 12, 15
h/d	1.5, 1.3, 1.2
bottom	False bottom / true bottom
Number of cells	11.7×10^6 / 8.7×10^6

3.2 VALIDATION

The computational results were verified through comparison with the experimental results as detailed in this section.

First, the calculation results obtained in the false bottom condition are compared in Figure 8 and discussed accordingly. Generally, the calculation results were good agreement with the experimental results, although the Y' and N' values obtained by the CFD simulation were underestimated when β was greater than 10°. These tendencies may be caused by the difference in hull attitude in the experimental and calculated scenarios.

Figure 9 shows the experimental and computational results measured in the true bottom condition. The absolute value of X' obtained by the CFD simulation was in good agreement with the experimental results, except for β=±15°. On the other hand, the absolute values of Y' and N' were smaller than those obtained from the experimental results when β was greater than 9°. For example, the differences between the experimental and computational results for h/d=1.2 at β=12° were 21% for Y' and 29% for N'. These tendencies are likely related to hull attitude, as was the case for the false bottom condition.

Finally, the false bottom effect was investigated by comparing the CFD simulation results in the false bottom and true bottom conditions, as shown in Figure 10. For X', the false bottom effect was not significant when β was less than 9°, but the absolute value of X' calculated in the false bottom condition was larger than that calculated in the true bottom condition when β was greater than 9°. This tendency is similar to the experimental results as discussed in Section 2.4. The values of Y' and N' in the false bottom condition were less than those in the true bottom condition. For example, the difference between the false bottom and true bottom conditions for h/d=1.2 at β=12° was 25% for both Y' and N', a smaller difference than indicated by the experimental results discussed in Section 2.4. However, the CFD simulation effectively captured the general tendency of the false bottom effect (the decrease in Y' and N' when measured in the false bottom condition) observed in experimental results.

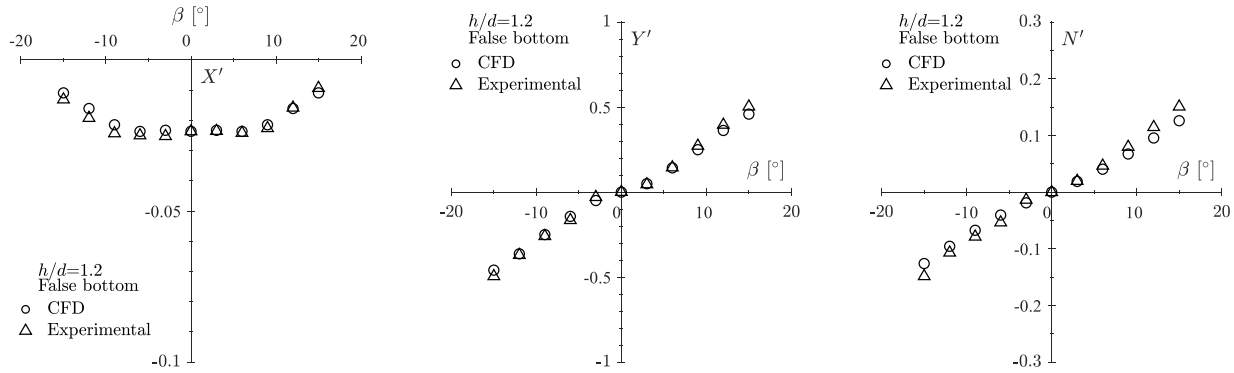

Figure 8. Comparison of the experimental and computational non-dimensional surge force, lateral force, and yaw moment obtained in the false bottom condition for h/d=1.2

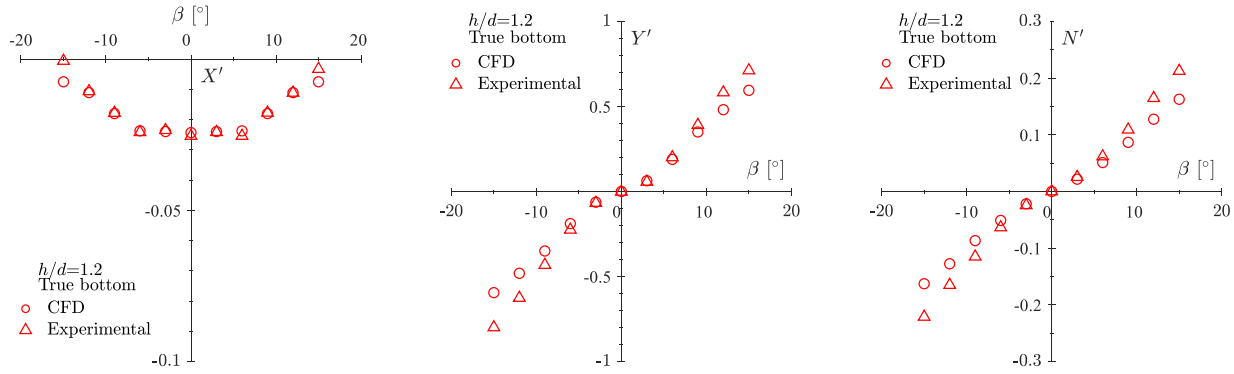

Figure 9. Comparison of the experimental and computational non-dimensional surge force, lateral force, and yaw moment in the true bottom condition for h/d=1.2

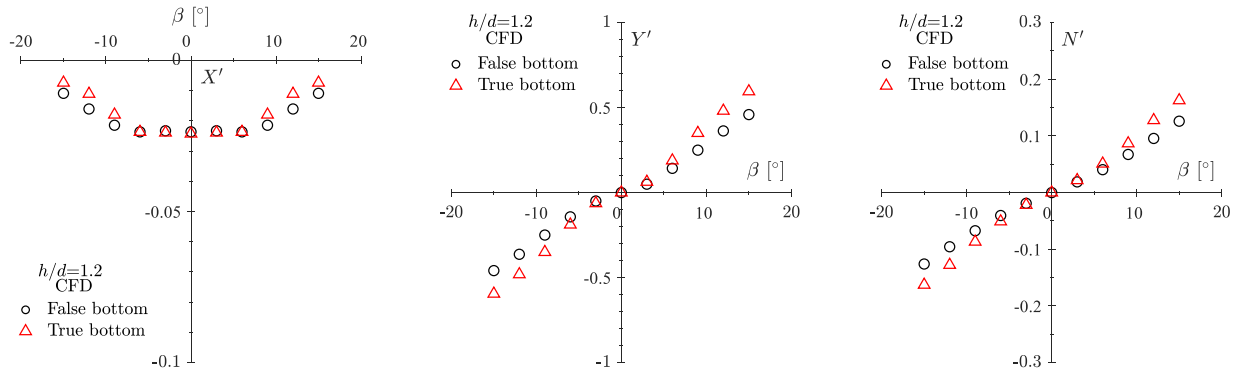

Figure 10. Comparison of the non-dimensional surge force, lateral force, and yaw moment obtained by CFD in the false bottom and true bottom conditions for h/d=1.2

3.3 LONGITUDINAL DISTRIBUTION OF LATERAL FORCE AND PRESSURE DISTRIBUTION ON THE HULL

The mechanism of the false bottom effect on Y' and N', which can be observed in both the experimental and computational results presented in this paper, is discussed in this section using the CFD results. First, the longitudinal distribution of the lateral force ($\Delta Y'$ distribution) is compared in Figure 11 in the false bottom and true bottom conditions for h/d=1.2 at β=6° and 12°. In the figure, the horizontal axis is the non-dimensional longitudinal coordinate x', where x'=0 indicates midship and x'=0.5 and -0.5 indicate fore perpendicular (F.P.) and aft perpendicular (A.P.), respectively. The total lateral force (Y') and total yaw moment around the midship (N') were then obtained by integrating $\Delta Y'$ and $x'\Delta Y'$, respectively, along x'.

The results show that the $\Delta Y'$ distribution in the false bottom condition is smaller than that in the true bottom condition. This difference is significant in the section from x'=-0.2 to x'=0.5. This tendency is consistent with the observed decreases in Y' and N' in the false bottom condition. In summary, the decrease observed in Y' and N' in the false bottom condition is related to the different magnitudes of $\Delta Y'$ acting on the hull from x'=-0.2 to x'=0.5.

Next, the pressure coefficient (C_p) distribution on the hull surface was compared for different bottom conditions; C_p is defined as $p/(0.5\rho U^2)$, in which p indicates the fluid dynamic pressure. In the figures, longitudinal coordinate is separated by nine square stations (S.S.1-S.S.9).

Figure 12 and 13 show the C_p distribution for h/d=1.5 and h/d=1.2 at β=6°, respectively. For h/d=1.5, no difference in the C_p distribution was obvious in the false bottom and true bottom conditions on either the port or starboard sides of the hull. However, obvious differences can be observed for h/d=1.2. On the port side (the side facing the flow), the positive pressure area (red area) stretching from F.P. to S.S.9 is clearly weaker in the false bottom condition than in the true bottom condition, whereas the false bottom effect is not obvious from S.S.9 to A.P. On the starboard side (which is the back side of the flow), the negative pressure area (blue area) in the false bottom condition is weaker than that in the true bottom condition from S.S.8 to S.S.3.

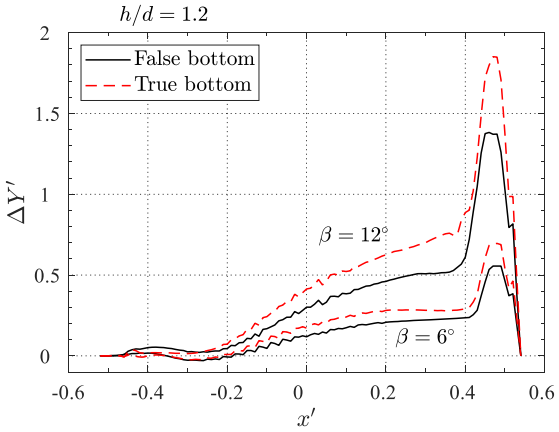

Figure 11. Comparison of the longitudinal distributions of lateral force acting on the hull in the false bottom and true bottom conditions at different drift angles for h/d=1.2

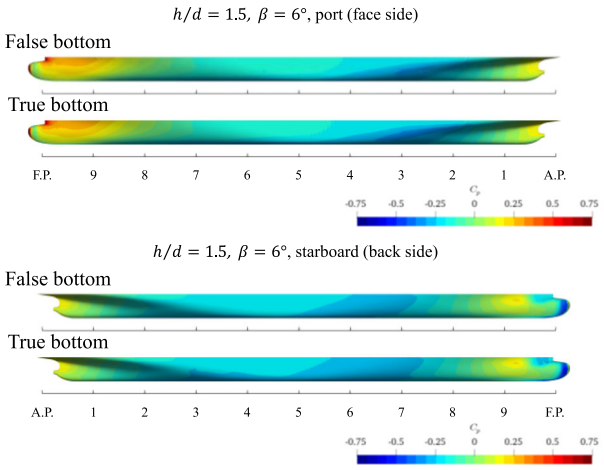

Figure 12. Comparison of the pressure coefficient distributions on the hull surface in the false bottom and true bottom conditions for h/d=1.5 at β=6°

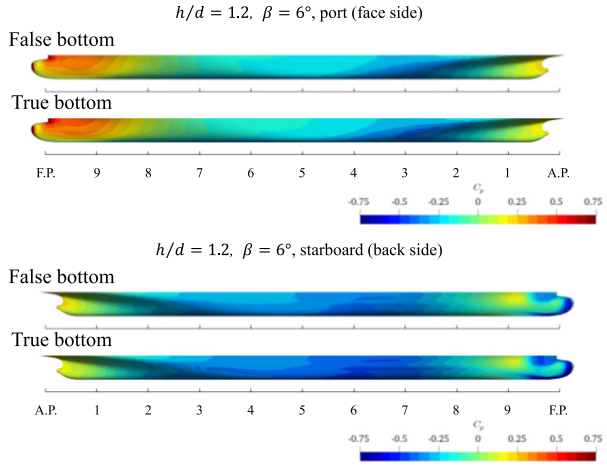

Figure 13. Comparison of the pressure coefficient distributions on the hull surface in the false bottom and true bottom conditions for h/d=1.2 at β=6°

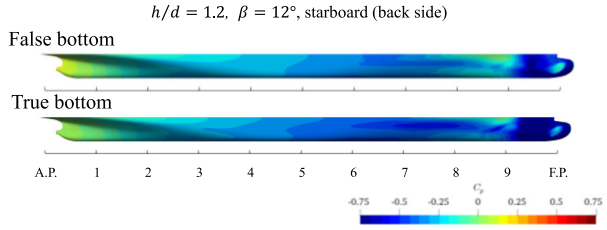

Figure 14. Comparison of the pressure coefficient distributions on the hull surface of the starboard side in the false bottom and true bottom conditions for h/d=1.2 at β=12°

Focusing on the back side of the hull where a significant difference was observed in the false bottom and true bottom conditions in Figure 12 and 13. Figure 14 shows the C_p distribution for h/d=1.2 and at β=12°. As shown in the figure, the difference in the negative pressure area with the false bottom and true bottom from S.S.8. to S.S.3 is significant compared to β=6°.

In summary, the negative pressure from S.S.8. to S.S.3 in the false bottom condition was found to be underestimated compared to that observed in the true bottom condition. This underestimate became significant with decreasing water depths and increasing drift angles. It is suggested that this difference is related to the false bottom effect on Y' and N'.

3.4 PRESSURE FIELD AROUND THE HULL

In this section, the pressure field around the model hull in the false bottom condition is compared with that in the true bottom condition to determine the cause of the underestimated negative pressure on the hull surface discussed in Section 3.3. Figure 15 and 16 show the C_p distribution around the hull, in which z_0/d =0.5 at h/d =1.2 is visualized. The black lines in the figures indicate the edges of the false bottom. In the true bottom condition, the negative pressure area on the back side of the hull expands in the y_0 direction with increasing drift angle. However, in the false bottom condition, the same expansion of the negative pressure area in the y_0 direction is insignificant.

To understand the relationship between the negative pressure area and width of the false bottom, the C_p distribution in the y_0-z_0 plane around the false bottom and true bottom is compared in Figure 17 and 18 at β=6° and 12°, respectively. In the figures, the C_p distribution around the hull at midship (x_0/L = 0.0) is visualized. In the true bottom condition, the negative pressure area can be observed to have developed widely, i.e., $y_0/(B_f/2)$ >1.6. However, in the false bottom condition, the negative pressure area is terminated near $y_0/(B_f/2)$ =1.0, which is the location of the edge of the false bottom. This tendency was confirmed for both β=6° and 12°.

In summary, in the false bottom condition, the negative pressure around the back side of the hull cannot be expanded in the y_0 direction owing to the limited width of the shallow water area. This caused the observed difference in the negative pressure on the hull surface and decrease in the Y' and N' (the false bottom effect).

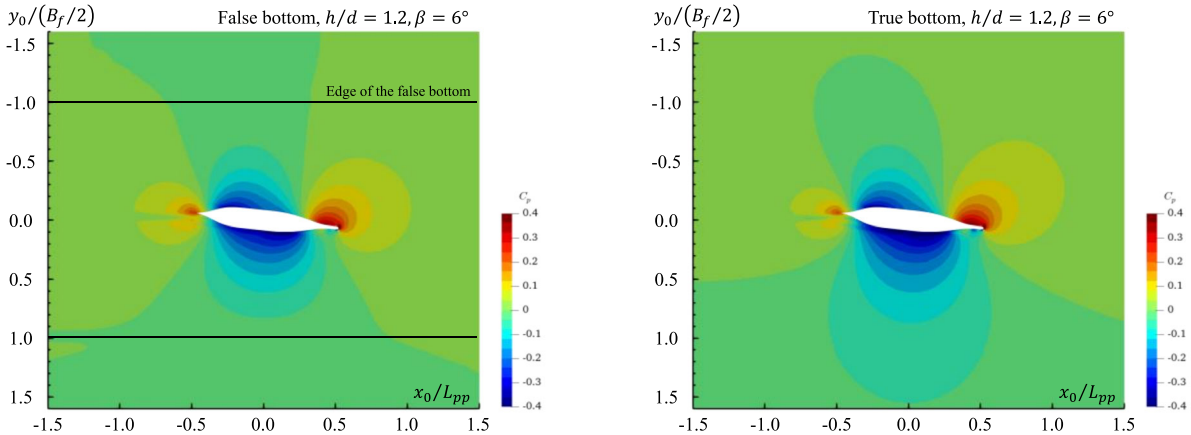

Figure 15. Comparison of the pressure coefficient distribution around the hull in the false bottom and true bottom conditions in the x_0-y_0 plane for h/d=1.2 at $z_0 = 0.5d$ and β =6°

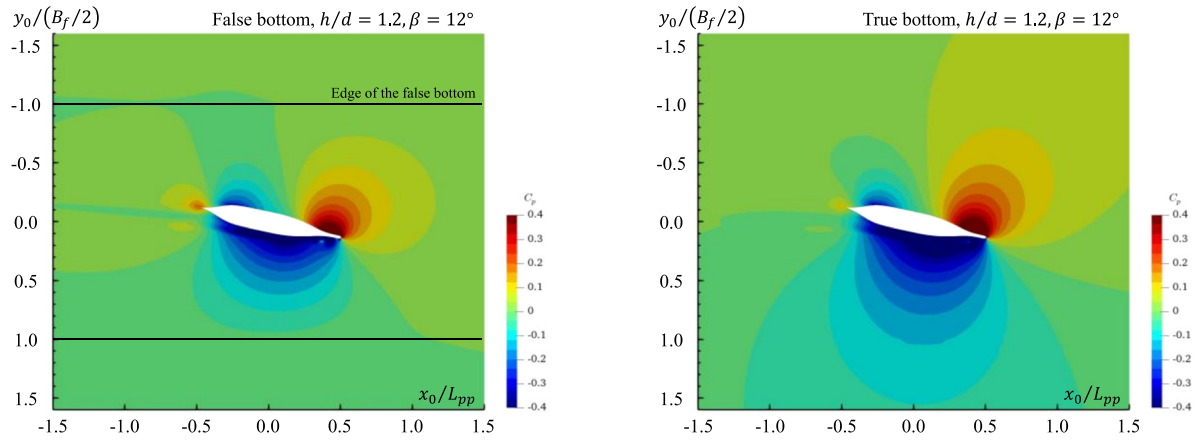

Figure 16. Comparison of the pressure coefficient distribution around the hull in the false bottom and true bottom conditions in the x_0-y_0 plane for h/d=1.2 at $z_0 = 0.5d$ and β =12°

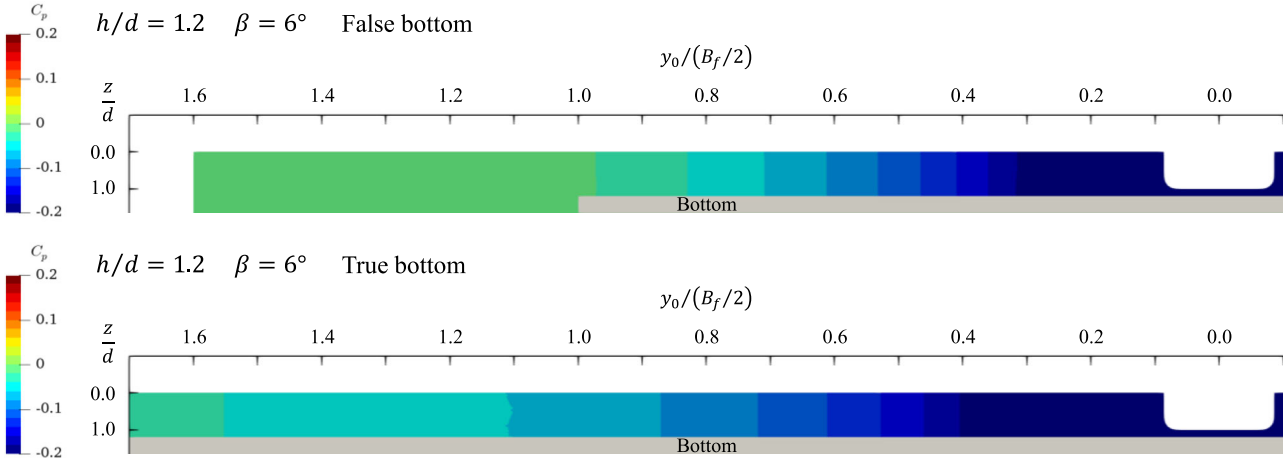

Figure 17. Comparison of the pressure coefficient distribution around the hull in the false bottom and true bottom conditions in the y_0-z_0 plane for h/d=1.2 at x_0/L_{pp}=0.0 and β =6°

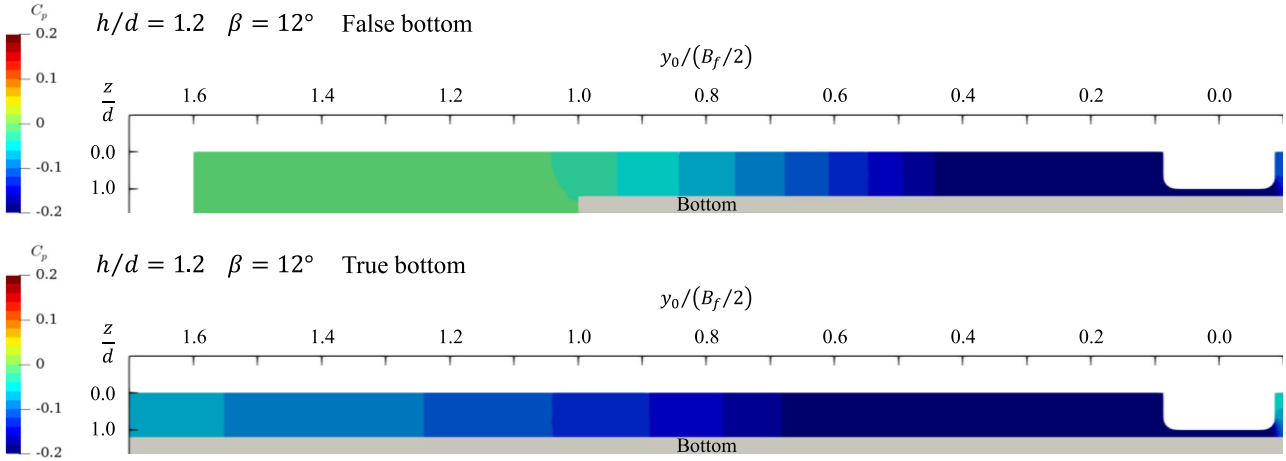

Figure 18. Comparison of the pressure coefficient distribution around the hull in the false bottom and the true bottom conditions in the y_0-z_0 plane for h/d=1.2 at x_0/L_{pp}=0.0 and β =12°

4 COUNTERMEASURES AGAINST THE FALSE BOTTOM EFFECT

Methods for improving the ability of the hydrodynamic forces measured in the false bottom condition to reflect the true bottom condition are discussed in this section. A countermeasure is suggested based on the flow field around the edges of the false bottom, and its applicability is discussed. An analytical correction countermeasure is also proposed and demonstrated.

4.1 FLOW FIELD AROUND THE EDGE OF THE FALSE BOTTOM

In this section, the flow velocity around the edge of the false bottom is discussed to inform a countermeasure against the false bottom effect.

Figure 19 shows the velocity profile in the y_0 direction (u_y) at $y_0/(B_f/2) = \pm 1$, which is the edge of the false bottom, at midship (x_0/L=0) for h/d=1.2 at β=6°. In the figure, (a) and (b) are located at $y_0/(B_f/2) = 1$ and $y_0/(B_f/2)$ =-1, respectively; these locations are indicated by the red lines in Figure 20. The arrows in Figure 19 show the flow velocity vectors in the false bottom condition projected on the y_0-z_0 plane.

In both the false bottom and true bottom conditions, the profiles in Figure 19 show that the flow is in the negative direction along the y_0 axis above the bottoms. This lateral flow is larger above the false bottom than above the true bottom. On the other hand, the flow is in the positive direction along the y_0 axis below the false bottom. These results indicate that the flow circulates around the false bottom. Thus, when viewed from ahead of the ship, the flow rotates in a clockwise direction around the false bottom (around the x_0 axis) when β is positive, and the opposite is true when β is negative. In this study, this flow is called "circulating flow".

Next, the relationship between the circulating flow and the hull inflow angle is investigated. In this study, a new physical value, the effective drift angle $\beta_{\text{Effective}}$, is introduced to consider the effect of the circulating flow on the hull inflow angle; $\beta_{\text{Effective}}$ is obtained from the geometrical drift angle β according to the following expression:

$$\beta_{\text{Effective}} = \beta - \tan^{-1}(\overline{u_y}/\overline{u_x}) \quad (1)$$

where $\overline{u_x}$ and $\overline{u_y}$ indicate the x_0 and y_0 components of the hull inflow velocity, respectively. In this study, $\overline{u_x}$ and $\overline{u_y}$ were obtained by spatially averaging from -1.5L_{pp} to 1.5 L_{pp} in the x_0 direction, from $-B_f/2$ to $B_f/2$ in the y_0 direction, and from 0 to h in the z_0 direction, as shown in Figure 21.

Figure 22 shows the relationships between β and $\beta_{\text{Effective}}$ in the false bottom and true bottom conditions. If $\beta_{\text{Effective}}$ is equal to β (as shown by the black dotted line), the conditions can be considered ideal for an oblique towing test. The figures show that $\beta_{\text{Effective}}$ is approximately the same as β in the true bottom condition regardless of the water depth. However, $\beta_{\text{Effective}}$ is consistently smaller than β in the false bottom condition and decreases more significantly with decreasing water depth because the circulating flow around the false bottom increases the $\overline{u_y}$, in turn increasing $\tan^{-1}(\overline{u_y}/\overline{u_x})$ and thereby decreasing $\beta_{\text{Effective}}$ as per the relationship in Eq. (1).

In summary, the circulating flow present in the false bottom condition decreases the effective drift angle ($\beta_{\text{Effective}}$) compared to the geometrical drift angle (β). Therefore, blocking this circulating flow represents a promising countermeasure against the false bottom effect.

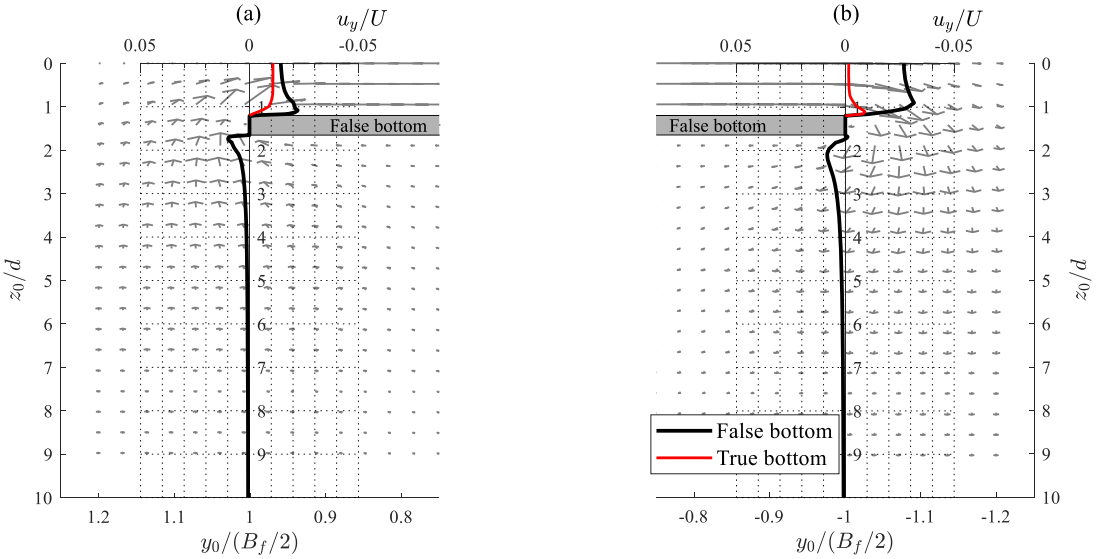

Figure 19. Velocity profile in the z_0-direction along the edge of the false bottom at midship (x_0/L_{pp} =0.0) for h/d=1.2 at β=6° viewed from ahead of the ship at: (a) $y_0/(B_f/2)$ =1 and (b) $y_0/(B_f/2)$ =-1 (Arrows indicate flow velocity vectors in the false bottom condition projected on the y_0-z_0 plane.)

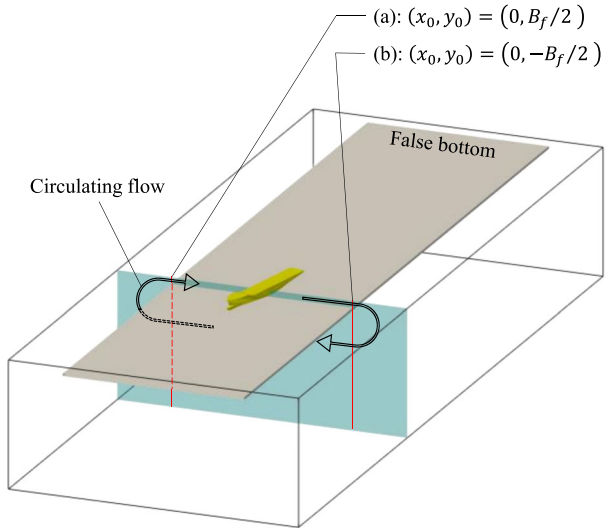

Figure 20. Schematic of the circulating flow and locations of (a) and (b) in Figure 19

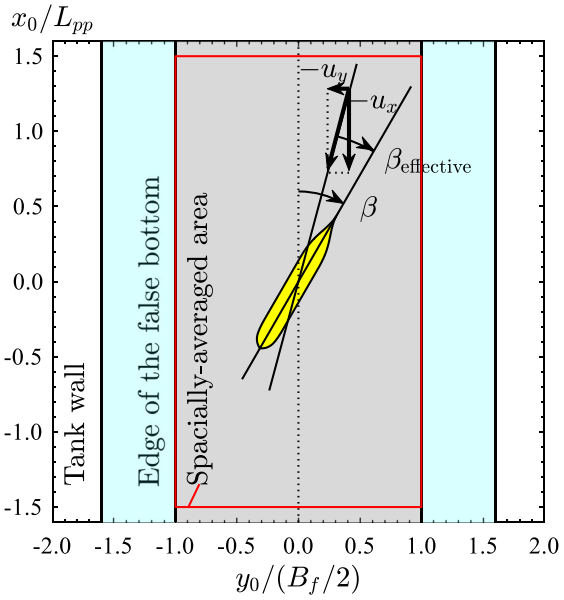

Figure 21. Schematic of the effective drift angle and spatially-averaged area

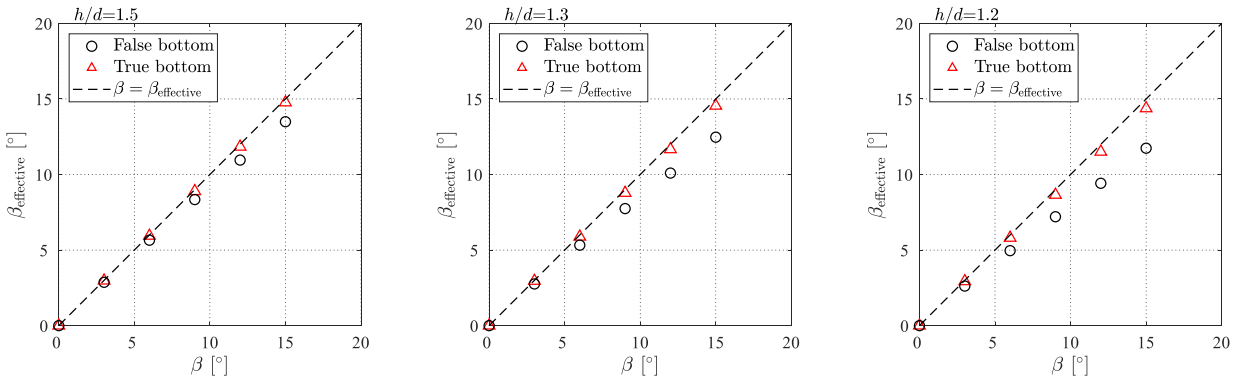

Figure 22. Comparison of the effective drift angle $\beta_{\text{Effective}}$ in the false bottom and true bottom conditions with different water depths obtained by spatially averaging the flow velocity around the hull (Averages are: $-1.5L_{pp} \leq x_0 \leq 1.5L_{pp}$, $-0.5B_f \leq y_0 \leq 0.5B_f$, $0 \leq z_0 \leq h$)

4.2 INSTALLATION OF A BLOCKING CURTAIN ALONG THE EDGE OF THE FALSE BOTTOM

Based on the analysis in Section 4.1, a method for blocking the circulating flow was developed, and its applicability is discussed in this section.

In this study, the relatively simple and practical approach of attaching a curtain along the edge of the false bottom was developed to block the circulating flow. This approach can be realized by attaching roller blinds to the edges of the false bottom, then lowering them to the tank bottom. In this study, this curtain is named the "blocking curtain" (BC).

A CFD simulation was conducted to evaluate the effectiveness and applicability of the BC. Figure 23 shows the computational domain. In this simulation, the BC was treated as a wall, and the calculation conditions were the same as those provided in Table 4.

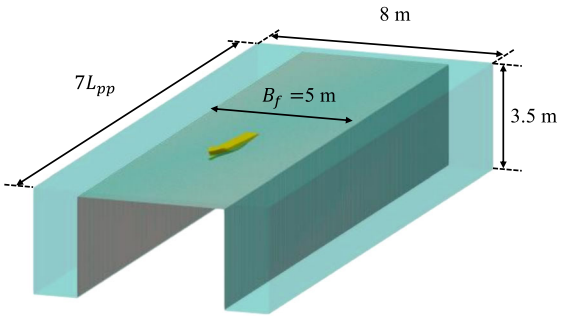

Figure 23. Computational domain with the blocking curtain (BC) attached to the edge of the false bottom

First, the effect of the BC on the flow velocity around the hull was analysed. Figure 24 shows the relationship between β and $\beta_{\text{Effective}}$ in the false bottom, true bottom, and false bottom with BC conditions. By attaching the BC, $\beta_{\text{Effective}}$ can be increased compared to the original false bottom condition. This indicates that the BC blocks the

circulating flow and reduces the lateral flow, then increases $\beta_{\text{Effective}}$.

Next, to confirm the applicability of the BC method, the hydrodynamic forces were compared. Figure 25 shows a comparison of X', Y', and N' in the false bottom, true bottom, and false bottom with BC conditions. By attaching the BC, the Y' and N' values increased compared to the original false bottom. When β was less than 6°, X', Y', and N' obtained in the false bottom with BC condition showed good agreement with those obtained in the true bottom condition. However, when β was greater than 9°, the absolute values of Y' and N' were relatively smaller than those in the true bottom condition. Thus, the proposed BC method increased Y' and N', but underestimated them compared to the results in the true bottom condition when β was large.

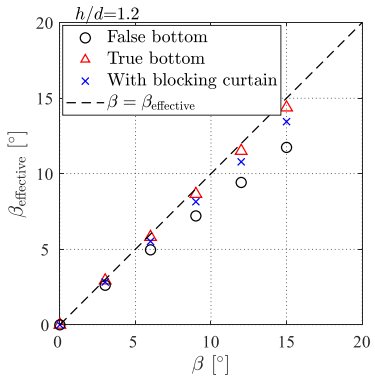

Figure 24. Comparison of the effective drift angle $\beta_{\text{Effective}}$ in the false bottom, true bottom, and false bottom with the blocking curtain conditions.

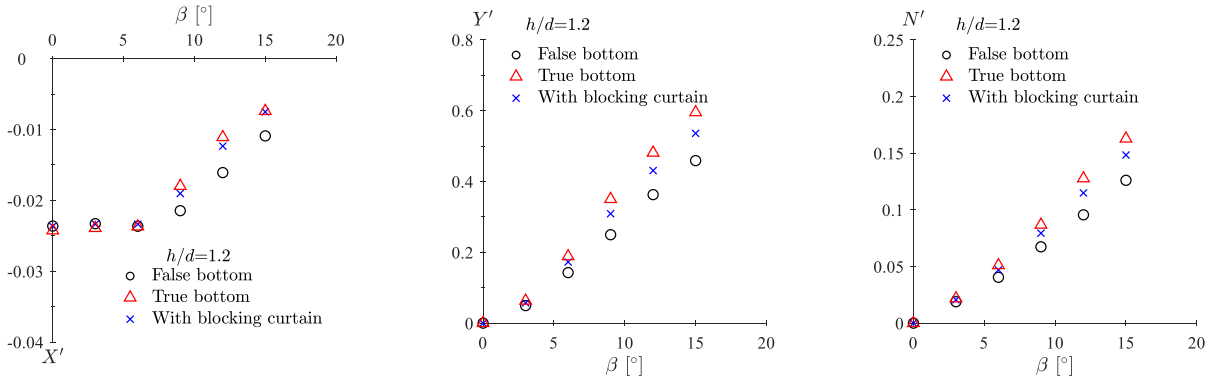

Figure 25. Comparison of the computational surge force, lateral force, and yaw moment of an obliquely moving ship in the false bottom, true bottom, and false bottom with a blocking curtain for h/d =1.2

4.3 HYDRODYNAMIC FORCE CORRECTION METHOD

In this section, an analytical method for considering the effect of the circulating flow on the hydrodynamic forces acting on the ship model is discussed. Instead of blocking the circulating flow, as with the BC method, this method converts β to $\beta_{\text{Effective}}$ using the following equation:

$$\beta_{\text{Effective}} = c_1 \beta \tag{2}$$

where c_1 is a correction coefficient that indicates the decrease in the drift angle. Table 5 shows the value of c_1 for each water depth in this study. These values were obtained by linear approximation of $\beta_{\text{Effective}}$ in Figure 22 for β and defining the coefficient of the first-order term as c_1.

Table 5. Correction coefficient for effective drift angle

h/d	1.5	1.3	1.2
c_1	0.884	0.816	0.775

To confirm the effectiveness of the analytical hydrodynamic force correction method, the hydrodynamic forces X', Y', and N' are compared in Figure 26 in the false bottom, true bottom, and hydrodynamic force-corrected conditions. By converting β to $\beta_{\text{Effective}}$ (reducing β according to Eq. (2)), X', Y', and N' in the false bottom condition were made to agree with the results calculated in the true bottom condition.

The correction coefficient c_1 is supposed to depend on many factors, e.g., the ratio of the ship size and false-bottom width, hull-drift angle, ship speed, etc. Therefore, a systematic study to investigate how much those factors influence on the hydrodynamic forces is required. This is one of the future works.

5 CONCLUSION

In this study, the effect of a false bottom tank on the hydrodynamic forces acting on an obliquely moving ship (the false bottom effect) was discussed. First, to understand the false bottom effect, captive model tests were conducted using a KCS model (bare hull) with L_{pp}= 3.057 m in false bottom (Hiroshima University towing tank) and true bottom (Kyushu University seakeeping and manoeuvring basin) conditions. Next, CFD simulations corresponding to each experiment were conducted to investigate the mechanism of the false bottom effect. The main conclusions of this study are as follows.

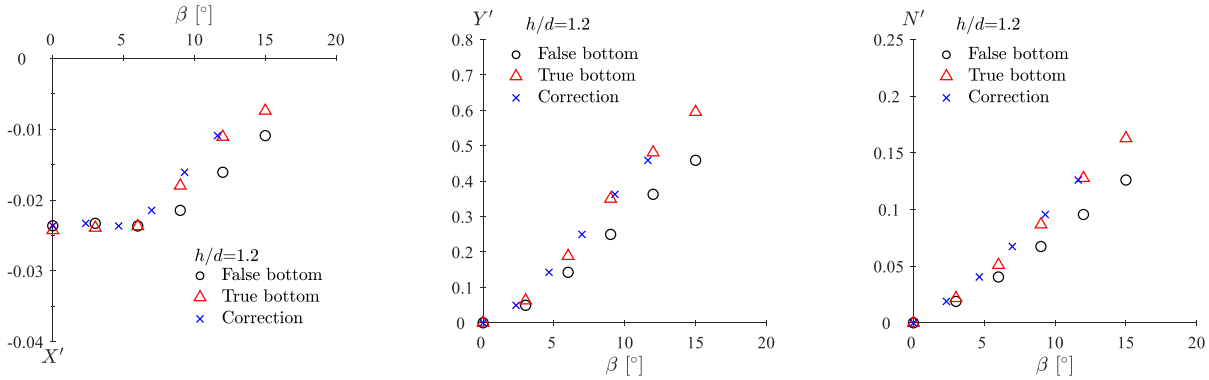

Figure 26. Comparison of the computational surge force, lateral force, and yaw moment of an obliquely moving ship in the false bottom, true bottom, and corrected (converting drift angle β to effective drift angle $\beta_{\text{effective}}$) conditions for h/d =1.2

- The experimental results showed that the absolute values of the lateral force Y' and yaw moment N' in the false bottom condition were smaller than those in the true bottom condition. This tendency was more significant as the water depth to draft ratio decreased from h/d=1.5 to h/d=1.2. For example, the values of Y' and N' measured in the false bottom condition for h/d=1.2 at β=12° were 47% and 43% smaller, respectively, than those measured in the true bottom condition.

- The CFD simulation results captured the tendency of the false bottom effect observed in the experiments. The pressure field distribution (C_p distribution) around the hull showed that the negative pressure area, which developed on the back side of the flow (starboard side when β is positive), was terminated near the edge of the false bottom. This caused the observed difference in the C_p distribution on the hull surface and the smaller absolute values of Y' and N'compared to the true bottom condition.

- As the circulating flow around the false bottom, which decreased with hull inflow angle, was responsible for the false bottom effect, two countermeasures against this effect were evaluated. The first method attached a blocking curtain to the edge of the false bottom to block the circulating flow from beneath. This increased the absolute values of Y' and N' but underestimated them compared to the true bottom condition when β was larger than 9°. The second method mathematically corrected the hydrodynamic forces by converting β to the effective drift angle $\beta_{\text{Effective}}$. This method can be applied to a range of β values from 0° to 15°, but detailed studies on the use of this correction coefficient are still required.

In this study, CFD simulations were conducted in steady-state condition and neglected the free surface effect and the change of the running hull attitude such as sinkage and trim. Therefore, more advanced numerical simulations are required to investigate the mechanism of the effect of the false bottom on the hydrodynamic forces in more detail. In addition, the experimental verifications should be conducted with respect to the countermeasure to attach the blocking curtain along the edge of the false bottom, as suggested in Section 4.2. A systematic investigation of the correction coefficient discussed in Section 4.3 is also one of the future works, e.g., the effect of the ratio of the ship size and false-bottom width, tank width, hull-drift angle, and ship speed on the correction coefficient.

6 ACKNOWLEDGEMENTS

We would like to express our gratitude to Mr. M. Dobashi, of Hiroshima University and Mr. H. Ibaragi of Kyushu University for supporting the tank tests in shallow water. We would also like to thank Assoc. Prof. T. Nakashima of Hiroshima University and Mr. S. Yagyu for their useful discussions. The computation in this study was carried out using the computer resources offered under the General Projects category by the Research Institute for Information Technology, Kyushu University. We would like to thank Editage (www.editage.com) for English language editing.

7 REFERENCES

Fujino, M., Ishiguro, T., 1984, A study of the mathematical model describing manoeuvring motions in shallow water, J. Society of Naval Architects of Japan 156, pp.180-192 (in Japanese)

Menter, F.R., Kuntz, M., Langtry, R., 2003. Ten years of industrial experience with SST turbulent model, Turbulence, Heat and Mass Transfer 4, pp.625-632

Sakamoto, N., Kobayashi, H., Ohashi, K., 2020. Overset RaNS Study for the Effect of False Bottom to the KCS under Static Drift in Shallow water, in: Proceedings of JASNAOE Annual Spring Meeting, Vol. 30, pp.569-574

Sakamoto, N., Ohmori, T., Ohashi, K., Kobayashi, H., 2021. Effect of False Bottom to the KCS under Pure Yawing Motion in Shallow Water (H/D=1.2) -Preliminary Study by Means of Viscous CFD-, in: Proceedings of JASNAOE Annual Autumn Meeting, Vol. 33, pp.193-198

SIMMAN, 2008. Part B: benchmark test cases, KCS description. In: Proceedings of Workshop on Verification and Validation of Ship Manoeuvering Simulation Methods (SIMMAN2008), Copenhagen, B11-B14

The 29th ITTC, 2021. System Manual, Recommended procedures and guidelines, Guideline on use of RANS tools for manoeuvring prediction, pp.1-17

The 29th ITTC, 2021. Technical Committee on Manoeuvring 2017-2021, in: Proceedings of 30th ITTC. https://ittc2021.com/homepage/proceedings/replay-of-the-live-sessions-from-14-to-18-june-2021-held-online
The OpenFOAM Foundation, 2016, OpenFOAM v5 User Guide, https://cfd.direct/openfoam/user-guide

Vantorre, M, Eloot, K., Delefortrie, G., Lataire, L., Candries, M., Verwilligen, J., 2017. Maneuvering in Shal-low and Confined Water, Encyclopedia of Maritime and Offshore Engineering

8 AUTHORS BIOGRAPHY

Yosuke HACHIYA is a master's course student at the Department of Transportation and Environmental Systems, Hiroshima University. He is responsible for research on ship manoeuvrability based on CFD calculations.

Masaaki SANO currently holds the position of associate professor at the Department of Transportation and Environmental Systems, Hiroshima University. He is responsible for research on ship manoeuvrability.

Ryusuke OKUDA is a doctoral candidate at the Department of Transportation and Environmental Systems, Hiroshima University. He is responsible for research on ship dynamics based on experimentation and simulation.

Yoshitaka FURUKAWA currently holds the position of professor at the Department of Marine Systems Engineering, Faculty of Engineering, Kyushu University. He is responsible for research and education regarding ship dynamics.

Hironori YASUKAWA currently holds the position of professor at the Department of Transportation and Environmental Systems, Hiroshima University. He is responsible for research on ship dynamics and hydrodynamic

9 APPENDIX: EFFECT OF THE TANK WIDTH ON THE HYDRODYNAMIC FORCES

The tank width of Hiroshima University (8 m) is different from that of Kyushu University (24 m). Figure A1 shows the computational results of X', Y', and N' in the cases of the false bottom (W=8 m, B_f=5 m), false bottom (W=24 m, B_f=5 m), and true bottom (W=24 m). It seems no significant difference in the hydrodynamic forces acting on the hull above 5 m-false bottom between the cases of 8 m- and 24 m-tank widths. This signifies that the effect of the tank width on the hydrodynamic forces would not be significant, at least in this case.

In reference to Figures 17 and 18, the negative pressure developed around the ship (blue area) does not reach to the tank wall in the false bottom case. It seems to disperse in the deep region around the false bottom. In the end, the similar results were achieved regardless of the tank width.

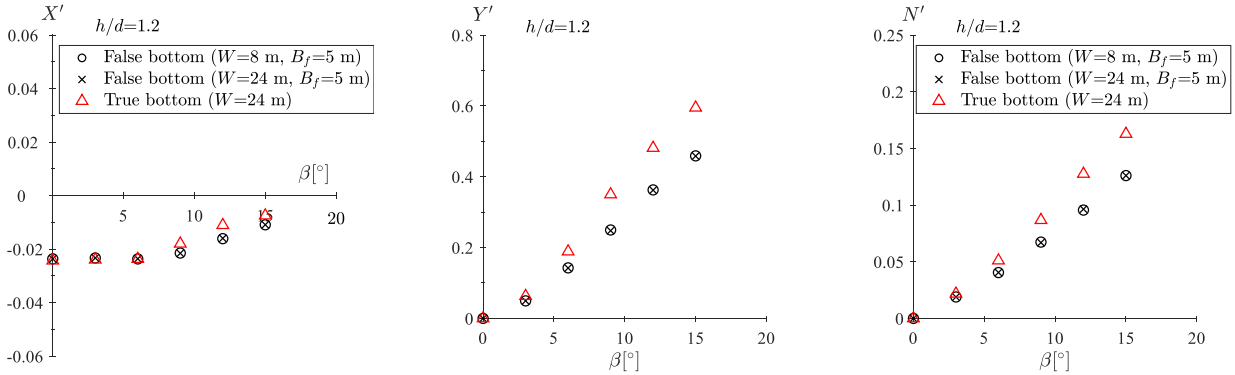

Figure A1. Comparison of the computational results of the non-dimensional surge force, lateral force, and yaw moment with the false bottom (W=8 m, B_f=5 m), false bottom (W=24 m, B_f=5 m), and true bottom (W=24 m) in h/d=1.2 (W and B_f indicate the width of the false bottom and tank width, respectively.)